

Modulation of Mitochondrial Bioenergetics by Polydopamine Nanoparticles in Human iPSC-Derived Cardiomyocytes

Syed Baseeruddin Alvi,[#] Divya Sridharan,[#] Mahmoud T. Shalaan, Shridhar K. Sanghvi, Muhamad Mergaye, Uzair Ahmed, Sarah K. Mikula, Harpreet Singh, and Mahmood Khan*

Cite This: <https://doi.org/10.1021/acsami.2c12575>

Read Online

ACCESS |

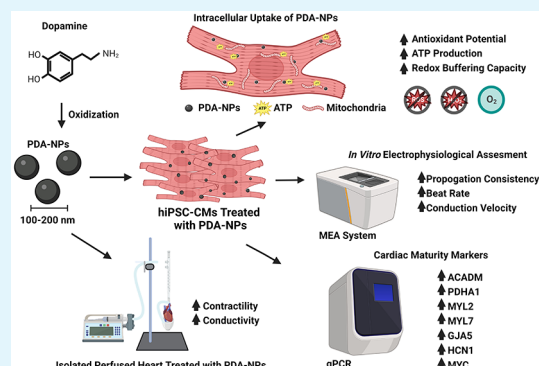
Metrics & More

Article Recommendations

Supporting Information

ABSTRACT: Myocardial infarction (MI) leads to the formation of an akinetic scar on the heart muscle causing impairment in cardiac contractility and conductance, leading to cardiac remodeling and heart failure (HF). The current pharmacological approaches for attenuating MI are limited and often come with long-term adverse effects. Therefore, there is an urgent need to develop novel multimodal therapeutics capable of modulating cardiac activity without causing any major adverse effects. In the current study, we have demonstrated the applicability of polydopamine nanoparticles (PDA-NPs) as a bioactive agent that can enhance the contractility and beat propagation of human-induced pluripotent stem cell-derived cardiomyocytes (hiPSC-CMs). Treatment of hiPSC-CMs with PDA-NPs demonstrated accumulation of the latter into mitochondria and significantly enhanced time-dependent adenosine triphosphate (ATP) production in these cells, indicating improved mitochondrial bioenergetics. Furthermore, the effect of PDA-NPs on hiPSC-CM activity was evaluated by measuring calcium transients. Treatment with PDA-NPs increased the calcium cycling in hiPSC-CMs in a temporal manner. Our results demonstrated a significant reduction in peak amplitude, transient duration, time to peak, and transient decay time in the PDA-NPs-treated hiPSC-CMs as compared to untreated hiPSC-CMs. Additionally, treatment of isolated perfused rat heart *ex vivo* with PDA-NPs demonstrated cardiogenic effects on the heart and significantly improved the hemodynamic function, suggesting its potential for enhancing whole heart contractility. Lastly, the gene expression analysis data revealed that PDA-NPs significantly upregulated cardiac-specific genes (ACADM, MYL2, MYC, HCN1, MYL7, GJA5, and PDHA1) demonstrating the ability to modulate genetic expression of cardiomyocytes. Taken together, these findings suggest PDA-NPs capability as a versatile nanomaterial with potential uses in next-generation cardiovascular applications.

KEYWORDS: heart failure, myocardial infarction, maturation, mitochondria, polydopamine



1. INTRODUCTION

Heart failure (HF) is a multifaceted bioenergetic disease characterized by poor cardiac contractility and low cardiac output. HF affects 26 million people worldwide and exerts a significant socio-economic burden.^{1,2} Myocardial infarction (MI) results from the blockage of the coronary artery supplying oxygenated blood to heart muscles causing damage to the ventricular muscle.³ The inflammatory response following MI exacerbates damage to the heart tissue by activating the cascade of matrix-metallo proteases (MMPs). MMPs' activation further results in ventricular wall thinning and remodeling.^{4,5} Taken together, all these events lead to the formation of a non-contractile scar tissue, hampering cardiac contractility leading to cardiac insufficiency, a reduction in the heart's ability to pump blood sufficiently. Current pharmacological interventions are limited in preventing cardiac remodeling, plausibly due to poor cardiac targeting.⁶ Despite recent advances, the current therapies for mitigating cardiac failure have not been successful in improving clinical outcomes.

At the molecular level, HF is strongly associated with impaired mitochondrial functioning. In HF, disturbances to mitochondrial bioenergetics cause a 30% decline in the adenosine triphosphate (ATP) production compared to healthy hearts.⁷⁻⁹ Therefore, the current pharmacological approach for HF treatment largely focuses on reducing the oxygen demand to compensate for the poor cardiac contractility.¹⁰ However, the next-generation therapeutics for HF are directed toward preserving cardiac functionality and enhancing the energy supply.¹¹ Another hallmark of HF is elevated Reactive Oxygen Species (ROS) levels due to alterations in the myocardial redox state.¹² Therapies targeting mitochondrial function, capable of

Received: July 14, 2022

Accepted: November 7, 2022

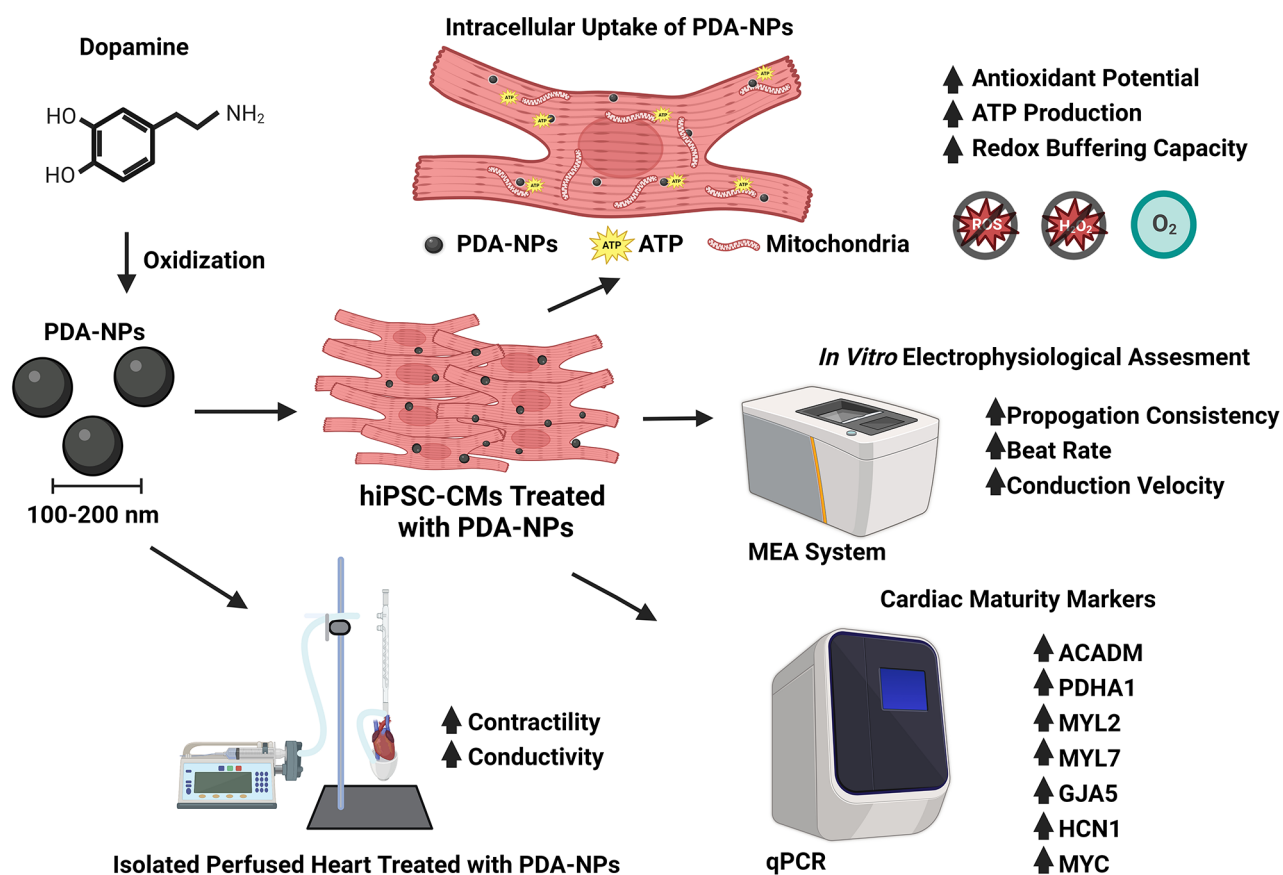


Figure 1. Schematic representing modulatory effect of polydopamine (PDA-NPs) on human induced pluripotent stem cell derived cardiomyocytes (hiPSC-CM's). The electrophysiological parameters of hiPSC-CMs treated with PDA-NPs were assessed using the multielectrode array system (MEA). The real-time measurement of H_2O_2 catalysis was assessed by Apollo free radical analyzer. The *ex vivo* analysis was performed on isolated hearts using the Langendorff apparatus. The expression of cardiac specific markers was evaluated by qPCR.

enhancing the ATP supply and redox buffering capacity, could emerge as promising therapies.^{13,14}

To address this long-standing problem, researchers have developed strategies involving biomaterials and nanomaterials as an alternative to current therapies. One of the most extensively studied material among them is polydopamine (PDA), also known as Mussel-inspired biomaterial. PDA exhibits a promising therapeutic potential due to its antioxidant, anti-inflammatory, immunomodulatory, and cardioprotective properties.^{15–18} It is well documented that PDA could effectively interact with a wide variety of surfaces due to the presence of adhesive catechol functional groups, which includes enhancing the wettability of coated scaffolds.¹⁹ Self-assembled PDA nanoparticles (PDA-NPs) have also been extensively studied for the application of drug delivery and light-mediated photothermal therapy, suggesting the growing interest in exploring PDA as a potential nanomedicine. However, there have been limited studies reported on PDA-NPs for their application as cardiac nanomedicine.

Nanoparticle-based therapies could emerge as a novel therapeutic intervention with enhanced site-specific effects and minimal off-target toxicities. Furthermore, nanoparticle-based therapies could also enable multimodal cardiac modulation effects.²⁰ In the current study, we have evaluated the potential of PDA-NPs in modulating the activity of human induced pluripotent stem cell-derived cardiomyocytes (hiPSC-CMs) (Figure 1). We hypothesize that PDA-NPs could demonstrate a dual response, primarily due to the superficial interaction with

the cell surface of the cardiomyocytes which may also alter the contractility and electrical conductivity of cardiomyocytes. Second, PDA-NPs can enhance mitochondrial ATP, thereby modulating mitochondrial redox buffering capacity.

2. MATERIALS AND METHODS

2.1. Materials. Dopamine HCl, Tris base, 2,2-Diphenyl-1-picrylhydrazyl (DPPH), and ascorbic acid were procured from Sigma-Aldrich. All the other reagents used were of analytical grade.

2.2. Culturing and Maintenance of hiPSC-CMs. The hiPSC-CMs were procured from Cellular Dynamics international (FUJIFILM Cellular Dynamics Inc.) and were cultured following the manufacturer's protocol as previously described.²¹ The plated cells were maintained in Cardiomyocyte Maintenance Medium (Fujifilm CDI) and incubated at 5% CO_2 in a humidified atmosphere at 37 °C.

2.3. Methods. **2.3.1. Preparation of PDA-NPs.** PDA-NPs were prepared by the oxidative polymerization of the dopamine monomer. Briefly, 60 mg of dopamine were weighed and dissolved in a mixture of water/ethanol (65 mL/60 mL) and stirred. To this mixture, 10 mL of water containing 90 mg of tris base were added, and the solution was stirred overnight. The change in color of the solution from light brown to black confirmed the formation of NPs. The following day, NPs were collected by centrifugation at 15,000 rpm for 10 min and lyophilized.²²

2.4. PDA-NPs Characterization. **2.4.1. UV-vis Spectroscopy, FTIR Spectroscopy, NTA and Zeta potential analysis.** The prepared nanoparticles were subjected to UV-vis spectroscopic analysis (Synergy H1, Biotek Instruments). The samples were diluted with water, and the absorbance spectrum was recorded from 400 to 900 nm. The FTIR (4500 portable FTIR spectrometer, Agilent) spectroscopic analysis was performed by drying the samples to form a film, and the

spectra were compared with free dopamine. For NTA (Nanosight NS-300, Malvern Analytical), the nanoparticle solution was diluted to a ratio of 1:1000, for evaluating the size distribution and nanoparticle concentration. Lastly, the nanoparticle samples were subjected to zeta-potential analysis to evaluate the surface charge.

2.4.2. TEM and SEM Imaging of PDA-NPs. The nanoparticles were imaged using Cryo-TEM (Thermo Scientific Glacios Cryo-TEM), and the samples were suspended in distilled water and casted on a copper grid for imaging. Similarly, for SEM (Apreo II) imaging, the samples were drop-casted on conductive carbon tape and gold sputter-coated prior to imaging.^{23,24}

2.4.3. Scanning Electron Microscopy (SEM) Imaging of PDA-NPs Treated Cardiomyocytes. The PDA-NPs (10 $\mu\text{g}/\text{mL}$) were exposed to hiPSC-CM's for 4 h on a glass coverslip, followed by the cells being washed with PBS and fixed using glutaraldehyde. The fixed cells were dehydrated by incubating them in ethanol gradually. Later the samples were sputter-coated and imaged using SEM (Apreo II).²⁵

2.4.4. Intracellular Uptake of PDA-NPs. Immunofluorescence imaging was performed on hiPSC-CMs cultured on coverslips. PDA-NPs were tagged with calcein by surface adsorption; briefly 1:1 (w/w) PDA-NPs and calcein were added to PBS (1 mL). The solution was stirred overnight, and the following day the pellet was collected and washed three times to avoid unbonded calcein. The hiPSC-CMs were incubated with PDA-NPs tagged with calcein (25 $\mu\text{g}/\text{mL}$) for 4 h after which they were washed twice with DPBS and processed for immunostaining as described previously.²⁶ Briefly, the cells were fixed in 4% PFA for 15 min at RT, permeabilized using 0.2% Triton X-100, and incubated in a blocking buffer containing 1% bovine serum albumin (BSA, Sigma-Aldrich, MO). The cells were incubated with the rabbit anti-Troponin T (1:200, Sigma-Aldrich, MO) overnight at 4 °C, followed by the anti-rabbit Alexa Fluor 594 (1:1000, Cell Signaling Technology, MA) for 1 h at RT in the dark. The cells were counterstained with DAPI (Thermo Fisher Scientific, MA), and the coverslips were mounted over glass slides using ProLong Gold Antifade Mountant (Life Technologies, MA). The cells were then imaged on an Olympus FV3000 (Olympus Life Sciences, PA) confocal microscope.

2.4.5. Mitochondrial Localization of PDA-NPs. The subcellular localization of PDA-NPs was evaluated by Immunofluorescence imaging as reported earlier.²⁷ Briefly, following a 24 h treatment with (10 $\mu\text{g}/\text{mL}$) PDA-NPs (calcein) the cells were washed fixed in 4% PFA for 15 min at RT. Permeabilization was done for 10 min at RT using 0.2% Triton X-100 and incubated in a blocking buffer containing 1% bovine serum albumin (BSA, Sigma-Aldrich, MO) for 1 h at RT. The cells were then incubated with Anti-ATP5A antibody [15H4C4]-Mitochondrial Marker, (abcam) at a dilution of 1:500 overnight at 4 °C, followed by Goat Anti-Mouse Alexa Fluor 647 antibody (abcam) at a dilution of 1:1000. The cells were counter stained with DAPI and mounted using ProLong Gold Antifade (ThermoFisher Scientific). The cells were imaged on an Olympus FV3000 microscope.

2.4.6. Isolated Mitochondrial Binding. The interaction of PDA-NPs with mitochondria was evaluated by isolating mitochondria from hiPSC-CMs. Mitochondria were isolated as described earlier.^{28,29} Briefly, hiPSC-CMs were homogenized in ice-cold mitochondrial isolation buffer (in mM/L, 70 sucrose, 210 mannitol, 1 EDTA- Na_2 , 50 Tris-HCl, pH 7.4) using a Potter-Elvehjem homogenizer (7 rapid strokes). The homogenate was transferred into a 2.0 mL Eppendorf tube and centrifuged at 2000 $\times g$ for 5 min. The supernatant was carefully transferred into a clean 1.5 mL Eppendorf tube and centrifuged at 12,000 $\times g$ for 10 min. The pellet containing crude mitochondria was suspended in 55 μL of resuspension buffer (70 mM sucrose, 210 mM mannitol, 0.1 mM EDTA- Na_2 , 50 mM Tris HCl, pH 7.4). The mitochondria were preincubated with 100 nM MitoTracker (ThermoFisher Scientific) for 60 min, and then incubated with PDA-NPs (10 $\mu\text{g}/\text{mL}$) for 4 h. They were imaged using a confocal microscope (Nikon AIR). The binding efficiency was calculated by using ImageJ.

2.4.7. Transmission Electron Microscopy (TEM) Imaging of PDA-NPs Treated Cells. The hiPSC-CMs were cultured on Permanox chamber slides (Sigma-Aldrich) at a density of 20,000 cells/well. The cells were treated with PDA-NPs (10 $\mu\text{g}/\text{mL}$) for 4 h. Later, the cells

were washed with PBS and fixed using glutaraldehyde (2%). Cells were then rinsed, and heavy metal stained using 2% aqueous osmium tetroxide followed by a rinse and 2% aqueous uranyl acetate. Cells were dehydrated using an ethanol dehydration series (70%, 90%, 100%) at 5 min for each step and four times for 15 min for the final step. Cells were then changed to acetone and infiltrated with an increasing series of EPON resin mix in acetone and subsequently embedded using inverted BEEM capsules at 60 °C for 24 to 48 h. After curing, the cells were then sectioned at 90–100 nm using a Leica ultramicrotome equipped with a Diatome histo diamond knife, and imaged using TEM (FEI Tecnai G2 Biotwin TEM).^{30,25}

2.4.8. Calcium Transient Imaging. For calcium imaging, 40,000 hiPSC-CMs were plated on fibronectin-coated glass-bottom dishes (Cellvis). Calcium transients in the hiPSC-CMs were visualized using the Fluo-4 AM (ThermoFisher Scientific) as per the manufacturer's instructions. Briefly, 0.5 mL of DMEM containing 10 μM of Fluo-4-AM dye was added to each dish, and the cells were incubated for 1 h at 37 °C in the dark. The medium was then replaced with fresh DMEM, and the cells were further incubated for 30 min before imaging in the line scan mode using a Nikon AIR HD laser-scanning confocal microscope. Calcium transients were recorded before and after the addition of 10 $\mu\text{g}/\text{mL}$ PDA-NPs. All acquired images were then analyzed using the ImageJ software to determine the changes in fluorescence intensity of the cells.

2.4.9. Multielectrode Array (MEA) Analysis of Cardiomyocytes. The field potentials of hiPSC-CMs treated with different concentrations of PDA-NPs were measured using an MEA system. For this, hiPSC-CMs were cultured at a density of 40,000 cells per well directly on 24-well MEA plates (M384-t MEA-24 W, Axion Biosystems, Atlanta, GA, United States) having 16 PEDOT microelectrodes per well for 2 weeks.³⁰ The plate was equilibrated in the MEA system (Maestro Edge, Axion Biosystems, Atlanta, GA, USA) for 30 min in 5% CO_2 with a humidified atmosphere at 37 °C. The baseline was recorded for each well for 5 min, after which the hiPSC-CMs were treated with different doses of PDA-NPs (5, 10, 25 $\mu\text{g}/\text{mL}$). The plates were equilibrated for 5 min after the addition of NPs, and the field potentials were recorded for 5 min. AxIS Navigator version 1.4.1.9 was used for data recording while the cardiac analysis tool version 2.1.10 (Axion Biosystems, Atlanta, GA United States) was used for data analysis. The beat period, field potential duration (FPD), and conduction velocity were calculated. Further, Fredericia's correction was applied to the FPD, to interpret the effect of PDA-NPs on the QT interval. All the electrophysiological parameters including Spike Amplitude Mean (SAM), Propagation Consistency (PC), and Beat Period Irregularity (BPI) were also calculated using AxIS Navigator (Axion Biosystems).

2.4.10. DPPH Assay. The antioxidant potential of PDA-NPs was evaluated by DPPH assay.³¹ A stock solution of DPPH (Sigma-Aldrich, USA) in ethanol was prepared (100 μM), and 100 μL from the stock solution were added to the 96-well plates. To each well nanoparticles in varying concentrations (1, 5, 10, 25, 50 $\mu\text{g}/\text{mL}$) were added, respectively. The decrease in absorbance following the addition of test samples was recorded, and the percent DPPH quenched was plotted. Ascorbic acid with the same concentration range was used as a control.

2.4.11. Catalytic Conversion of H_2O_2 by PDA-NPs. To assess the antioxidant potential of PDA-NPs, we monitored the catalytic conversion of H_2O_2 to oxygen in the presence of PDA-NPs.³² The measurement of H_2O_2 was done using Apollo 4000 free radical analyzer (World Precision Instruments, Sarasota, FL, USA). The Apollo system HPO probe was inserted in a sealed 25 mL bottle containing a 5 mL deoxygenated water suspension of PDA-NPs (10 $\mu\text{g}/\text{mL}$). The system recorded the decline of H_2O_2 concentration upon mixing with PDA-NPs. After switching to the O_2 probe, the same setup was used to record the concentration of oxygen generated by mixing 10 $\mu\text{g}/\text{mL}$ PDA-NPs with 1 mM H_2O_2 over a 24 h time course.

2.4.12. Assessment of Intracellular Quenching of H_2O_2 . The intracellular quenching of H_2O_2 was measured by using a commercially available kit (abcam). Briefly, the cells were grown in a 24 well plate coated with 0.1% gelatin with an approximate density of 30,000 cells/well. After 48 h of incubation, the cells were treated with PDA-NPs (10

and 25 $\mu\text{g/mL}$) for 24 h. Later, the cells were washed to remove excess nanoparticles and cells were treated with a H_2O_2 probe supplied in the kit at 1:20 dilution and incubated for 60 min. After this step, the cells were again given a gentle wash with the supplied buffer to remove excess dye. Followed by adding fresh media containing 100 μM H_2O_2 for 15 min. The fluorescence intensity was recorded by using a plate reader (Synergy H1, Biotek Instruments) and performing area scan at Ex: 543 nm and Em: 570 nm.³³

2.4.13. ATP Estimation. The ATP measurements were made using the ATP Bioluminescence Assay Kit HS II (Sigma-Aldrich). Briefly, the hiPSC-CMs were plated on a 6-well plate, the cells were treated with PDA-NPs at different time-points (0, 4, and 24 h). Following the treatment, cells were trypsinized and collected. The cells were lysed and reacted with luciferase for luminescence signal acquisition using the SpectraMax M4 Microplate Reader (Molecular Devices LLC).³⁴

2.4.14. Langendorff Isolated Perfused Heart Experiment. The Langendorff isolated heart perfusion experiment was performed by following the method as published earlier.³⁵ Briefly, Sprague–Dawley rats were anesthetized, hearts removed, and retrogradely perfused at constant 80 mmHg pressure using 95% O_2 /5% CO_2 bubbled modified Krebs buffer. A water-filled balloon catheter connected to a pressure sensor was inserted in the left ventricle below the left atria to record the LVSP, LVDP, and heart rate. Three-lead EKG micro clips were connected to the heart to acquire the electrical activity. The perfusion rate was monitored using an inline transonic flow probe connected to a T106 flow meter (Transonic systems, USA). All signals from the connected sensors were computer-acquired using Powerlab 4/20 (AD Instruments, USA) and LabChart 5 Software (5.5.6). All animal experiments were performed according to the guidelines of the Institutional Animal Care and Use Committee at The Ohio State University.

2.4.15. Gene Expression Analysis. RNA Isolation. hiPSC-CMs were cultured at 10 $\mu\text{g/mL}$ PDA NPs for 2 weeks. The cells were washed with PBS and lysed in TRIzol reagent (ThermoFisher Scientific, USA). The lysate was centrifuged at 13,000 rpm for 15 min, and the supernatant was collected. An equal volume of ethanol (100%) was added and mixed thoroughly. Total RNA was extracted using the Direct-zol RNA Miniprep kit per the manufacturer's protocol (Zymo Research, Irvine, CA). RNA was quantified using a NanoDrop 2000 spectrophotometer (ThermoFisher Scientific, USA) and stored at -80°C for further analysis.

cDNA Synthesis. First strand cDNA synthesis was performed using the Qiagen RT2 First Strand cDNA synthesis kit (330404, Qiagen) per the manufacturer's protocol as described previously.³⁰

Real-Time Quantitative PCR. RT-qPCR was performed using Qiagen RT2 SYBR green ROX qPCR Mastermix (330523, Qiagen) according to the manufacturer's protocol as previously described³⁰ on a QuantStudio 3 (Applied Biosystems, USA) using QuantStudio design and analysis software V.1.4.1. Data are expressed as mean \pm SD, $n = 3$.

3. RESULTS AND DISCUSSION

The Mussel-inspired PDA is formed by oxidative polymerization of dopamine. PDA-NPs have been extensively researched as a photothermal transducer for photothermal therapy of localized tumors. Recent literature strongly supports the use of polydopamine-hybrid constructs like PDA-CNTs,³⁶ PDA-MXene,³⁷ and PDA-rGO,³⁸ for tissue engineering applications pertaining to conductive cells like neurons and cardiomyocytes.^{39,40} In the current study we have evaluated the dynamics of intracellular and extracellular interactions of self-assembled PDA-NPs with hiPSC-CMs. The PDA-NPs were prepared by oxidative polymerization of the dopamine monomer. These nanoparticles exhibited a wide range of absorbance, characteristic of PDA-NPs (Figure 2A).⁴⁰ Both free dopamine and PDA-NPs were then subjected to FTIR analysis, and as shown in Figure 2B, the characteristic peaks at 3200 and 1650 cm^{-1} represent the $-\text{OH}$ and $-\text{NH}$ functional groups present in free dopamine. In contrast, the peak at 3200 cm^{-1} was relatively reduced in PDA-

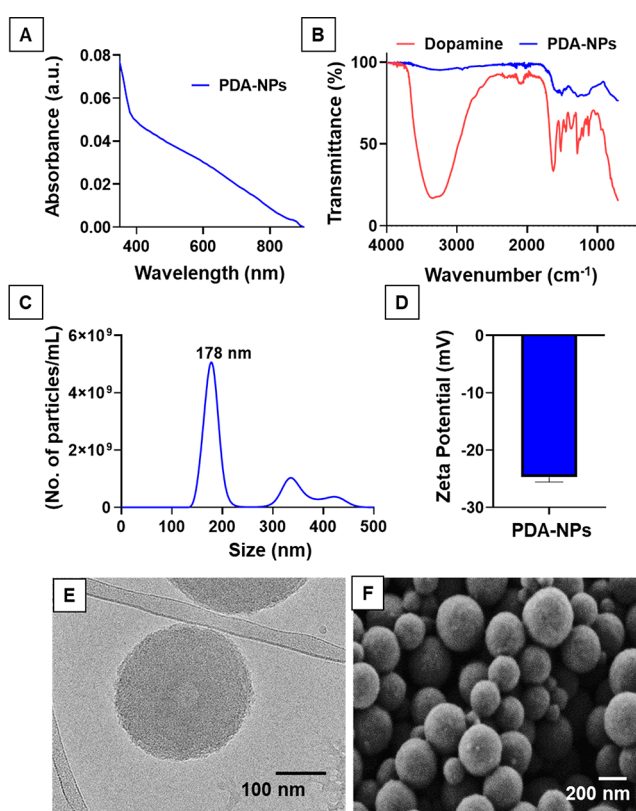


Figure 2. Physicochemical characterization of PDA-NPs. (A) UV–vis spectroscopic analysis of PDA-NPs. (B) FTIR spectroscopic analysis of dopamine and PDA-NPs. (C and D) NTA and Zeta potential analysis of PDA-NPs. (E and F) TEM and SEM imaging of PDA-NPs, respectively.

NPs. The presence of $-\text{OH}$ functional groups on PDA-NPs are responsible for the antioxidant properties. Later, the PDA-NPs were subjected to NTA analysis to evaluate the size distribution, and as shown in Figure 2C, PDA-NPs were around 180 nm, exhibiting a strongly negative zeta potential (Figure 2D). The prepared NPs were then subjected to SEM and TEM imaging revealing a solid and spherical nanostructure (Figure 2E,F).

To evaluate the cellular interaction of PDA-NPs with hiPSC-CMs, SEM imaging was performed on the cells post incubation (4 h). As shown in (Figure 3A–3C) the PDA-NPs were found to be adhering on the cell surface despite several wash cycles. These findings suggest that PDA-NPs could physically bind on the cell surface possibly due to the adhesive properties of PDA.⁴¹ The intracellular uptake of PDA-NPs loaded with calcein (Figure S1) was identified via confocal microscopy, and the hiPSC-CMs were immune-stained for troponin-T. Confocal images revealed that PDA-NPs accumulated within the cytoplasmic region of the cell (Figure 3D–3G). Furthermore, PDA-NPs treated cells were stained for mitochondrial-specific ATP5A to evaluate mitochondrial localization. As shown in Figure 4A–4I, the PDA-NPs were found to be in cytoplasm and associated with mitochondria. These results show that nanoparticles are present in the vicinity of mitochondria. However, to further confirm the binding of PDA-NPs to the mitochondria of the cardiomyocyte's, isolated mitochondria were loaded with mito-tracker and incubated with PDA-NPs. As shown in Figure 4J–4L, PDA-NPs were colocalized with isolated mitochondria. Protein proximity analysis²⁹ indicated that the colocalization index between NPs and mitochondria was $0.44 + 0.05$ ($n = 14$). Our results show

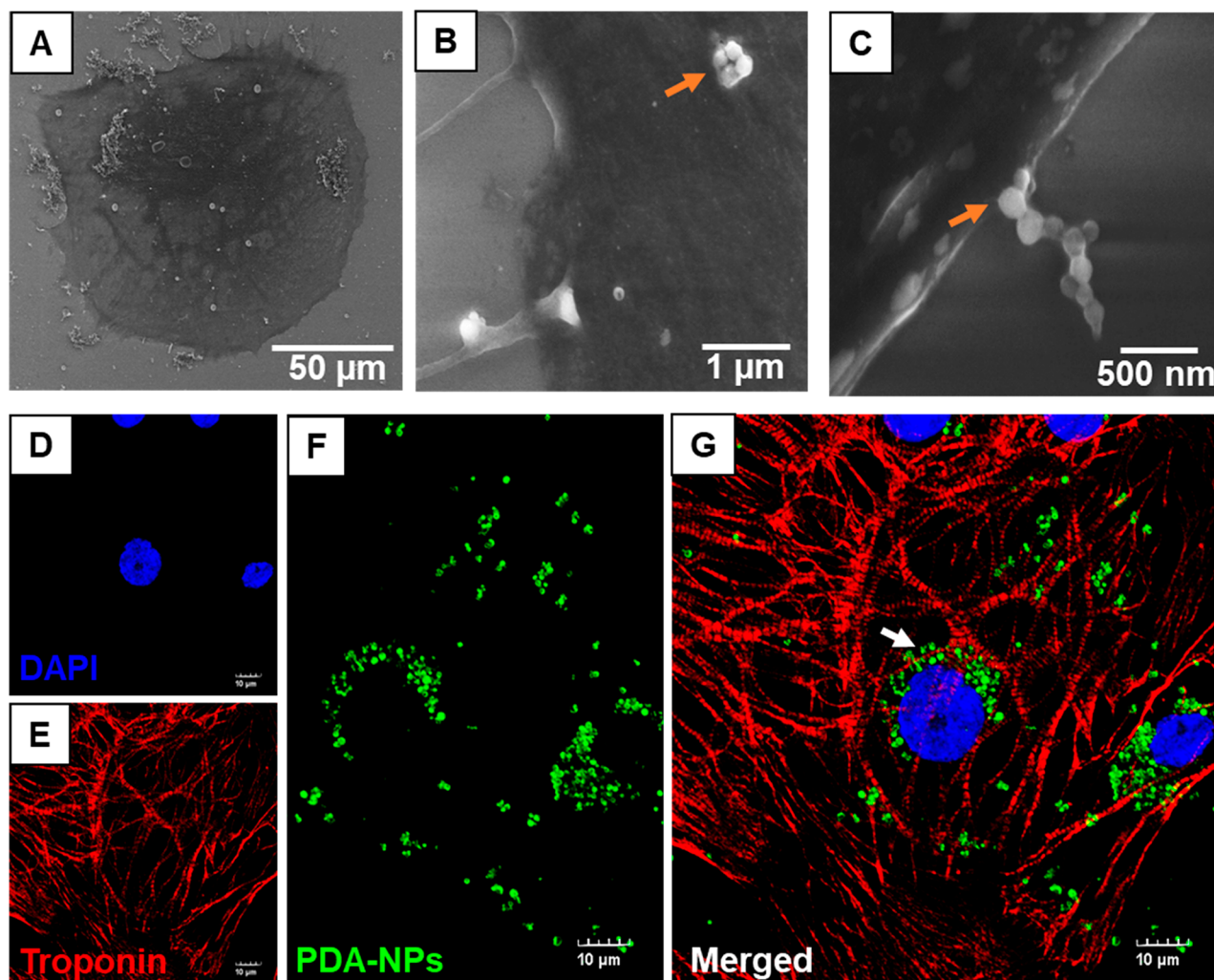


Figure 3. Extracellular and intracellular interaction of PDA-NPs with hiPSC-CM's. (A, B, and C) SEM images of PDA-NPs binding the hiPSC-CM's superficially (orange arrows). Intracellular uptake of PDA-NPs (D) DAPI, (E) Troponin T, (F) PDA-NPs labeled with calcein. (G) Merged image, white arrow shows PDA-NPs.

direct evidence of NPs and mitochondria interacting with each other. In cells, there are other organelles and cellular components present in the vicinity of mitochondria where NPs can localize. However, our approach of imaging isolated mitochondria rules out the role of any other cellular component in the interaction of nanoparticles and mitochondria.⁴² It should be noted that only ~45% of mitochondria isolated from cells interact with NPs (Figure S2). Furthermore, TEM imaging was performed on the hiPSC-CMs treated with PDA-NPs, and as shown in Figure 4M–4O, the PDA-NPs were observed in and around mitochondria with only smaller size PDA-NPs penetrating inside mitochondria. These findings confirm that the PDA-NPs exhibit mitochondrial binding.

The effect of PDA-NPs on hiPSC-CMs activity was evaluated by measuring calcium transients. Treatment with PDA-NPs enhanced the calcium transients in hiPSC-CMs in a time-dependent manner. As shown in Figure 5A–5D, a significant reduction in peak amplitude, transient duration, time to peak, and transient decay time was noted when compared to baseline. These results suggest that PDA-NPs could exhibit a drug-like effect on hiPSC-CMs, which can significantly modulate cardiac contraction (Figure 5E–5G). To further confirm the cardio-modulatory potential of PDA-NPs, we investigated the electro-

physiological changes in hiPSC-CMs using MEA analysis. The hiPSC-CMs cultured on MEA plates were treated with PDA-NPs in different doses (5, 10, and 25 $\mu\text{g}/\text{mL}$). The PDA-NPs treatment of hiPSC-CMs caused an immediate increase in the beat rate in a dose-dependent manner (Figure 6A). The enhanced contractility of cardiomyocytes was maintained in all treated wells for 48 h post-treatment. As shown in Figure 6B a significant dose-dependent decrease in the beat period was observed in PDA-NPs treated groups, when compared to the untreated group. These findings were consistent with a significant decline in field potential duration (FPD) in PDA-NP treated cardiomyocytes. As shown in Figure 6C, an increase in the dose of PDA-NPs leads to a significant decrease in FPD of hiPSC-CMs, suggesting enhanced conductivity. A significant shortening of the Q-T interval was also observed in a dose-dependent manner as shown in Figure 6D–6F (the black and red arrows represent the field potential before and after PDA-NPs treatment, respectively, showing significant shortening post-treatment). These results further correlate with the calcium transients suggesting modulation of cardiomyocyte contractility by PDA-NPs treatment. Further, we also monitored the treated wells for the parameters influencing the electrical conductivity of hiPSC-CMs as shown in Figure 7A. We found that with an

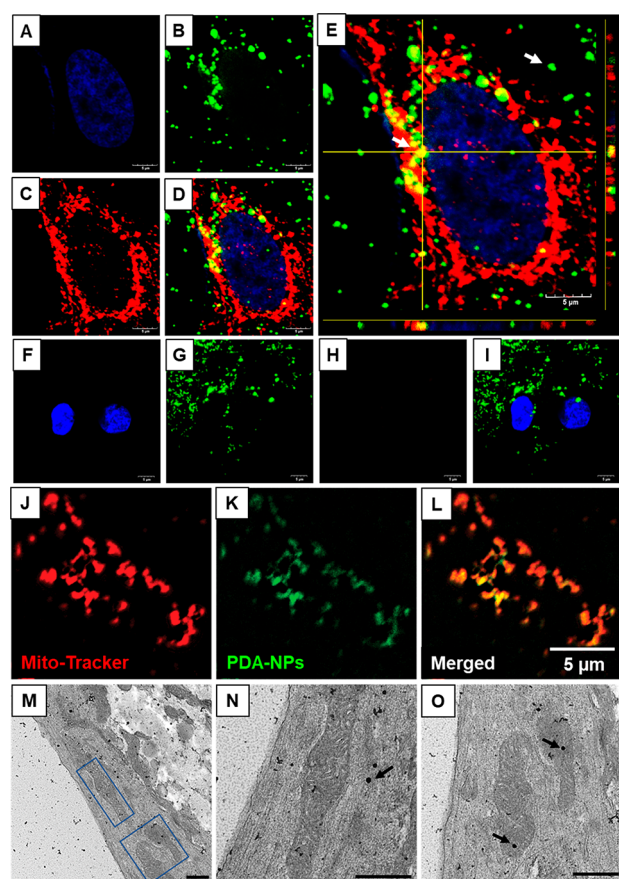


Figure 4. Intracellular localization of PDA-NPs and mitochondrial binding. (A) DAPI, (B) PDA-NPs (calcein), (C) Anti-ATP5A antibody (mitochondrial marker) + Secondary antibody Alexa Fluor 647, (D) Merged image. (E) 3-D Z-stacked image (white arrows showing the presence of PDA-NPs localized with mitochondria and in cytoplasm). Control (F), DAPI (G), PDA-NPs (calcein), (H) Secondary antibody, Alexa Fluor 647, (I) Merged image. (J) Mito-Tracker staining of isolated mitochondria. (K) PDA-NPs (calcein), (L) Merged image. (M) TEM images of PDA-NPs localizing to mitochondria of treated hiPSC-CMs. (N and O) Zoomed images of (M) respectively (black arrows showing PDA-NPs). Scale bar 500 nm.

increasing concentration of PDA-NPs from 5 to 25 $\mu\text{g}/\text{mL}$ a gradual increase in the mean spike amplitude was evident, suggesting that treatment with PDA-NPs enhances the depolarization of the cell (Figure 7B).⁴³ Furthermore, a similar response was observed in conduction velocity across the cell (Figure 7C). It is also worth mentioning that treatment with PDA-NPs also enhanced the beat propagation consistency and conductance (Figure 7D). On the other hand, a significant decline in the beat period irregularity was observed with PDA-NPs treatment (Figure 7E). Taken together, these findings suggest that PDA-NPs exhibit strong bioactivity on conductive cells like hiPSC-CMs and can modulate electrophysiological parameters influencing the function of these cells.

In chronic conditions like HF, where the electrophysiological parameters are adversely affected, intracellular stressors like ROS can exacerbate the cellular damage.⁴⁴ PDA-NPs are known to possess the antioxidant potential which have been widely reported.^{45,46} PDA-NPs were also assessed for free radical scavenging potential by DPPH assays. As shown in Figure S3, PDA-NPs demonstrated a significant free radical scavenging activity in a dose-dependent manner. At the dose of 10 $\mu\text{g}/\text{mL}$

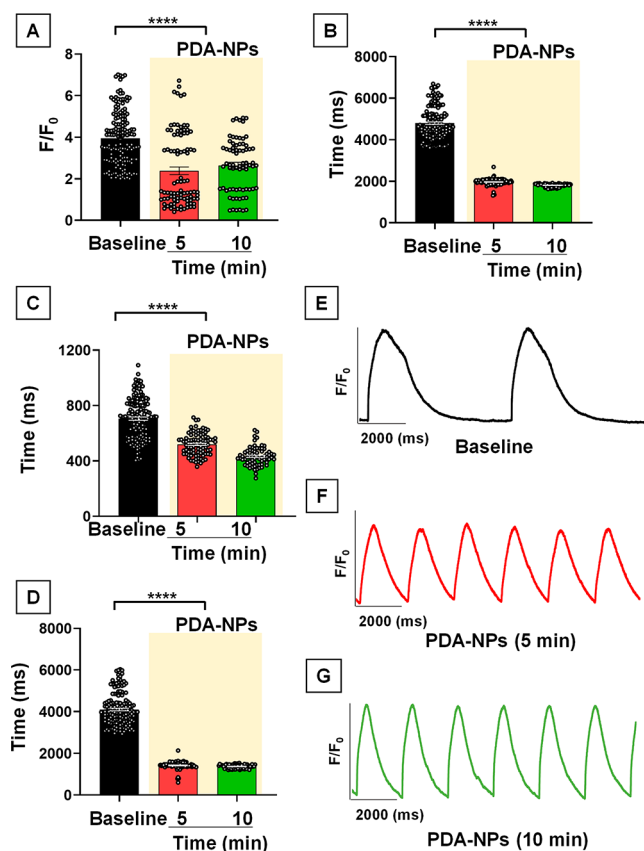


Figure 5. Calcium transients analysis post PDA-NPs treatment. (A and B) Peak amplitude and transient duration of hiPSC-CMs before PDA-NPs treatment and post-treatment (5 and 10 min) respectively. (C and D) Time to peak and transient decay before and after PDA-NPs treatment (5 and 10 min). (E, F, and G) Representative transient peak at baseline and post PDA-NPs treatment (5 and 10 min). Data represent Mean \pm SD. One-way ANOVA was performed followed by Dunnett's test for comparison with control, **** $P < 0.0001$.

about 60% of free radicals were quenched within 60 min of addition, whereas at 25 $\mu\text{g}/\text{mL}$ the scavenging activity of PDA-NPs was comparable to the case of ascorbic acid. We then tested the ability of PDA-NPs to quench intracellular ROS, and as shown in Figure S4A–B, pretreatment of hiPSC-CMs with PDA-NPs prevents excessive accumulation of ROS. Furthermore, untreated cells showed loss of activity due to the injury while PDA-NPs pretreated groups were functional (Figure S4C). These observations agree with the earlier published reports demonstrating the cytoprotective effect of PDA-NPs on cardiomyocytes.^{16,47}

The overwhelming accumulation of ROS generated due to the redox imbalance observed during disease state gets converted to H_2O_2 causing excessive cellular damage.⁴⁴ This could be mitigated by enhancing the redox buffering capacity of the cells. Next, we tested the catalysis of H_2O_2 by monitoring the real-time concentrations of H_2O_2 and O_2 . As shown in Figure 8A, an immediate reduction in H_2O_2 concentration was noted when compared to the control in the presence of PDA-NPs; these findings demonstrate the enzyme-like activity of PDA-NPs. Furthermore, As shown in Figure 8B, the generation of O_2 from H_2O_2 upon PDA-NP (10 $\mu\text{g}/\text{mL}$) treatment was significantly accelerated. When the PDA-NPs are exposed to H_2O_2 , it is known to degrade.⁴⁶ Therefore, we performed an accelerated degradation of PDA-NPs by adding varying

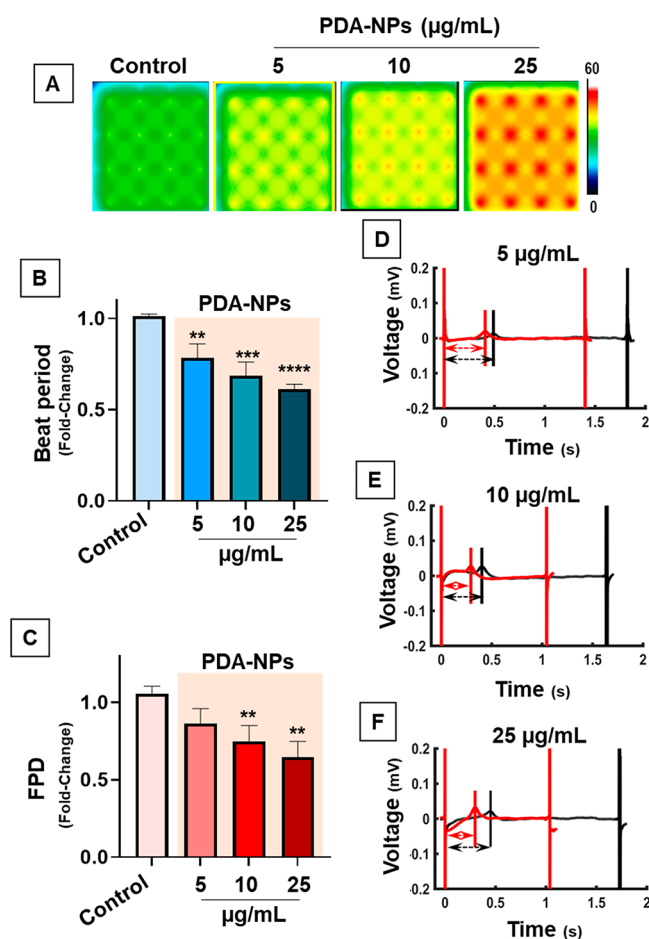


Figure 6. Multielectrode array analysis of PDA-NPs treated hiPSC-CMs. (A) Heat map showing the changes in beat rate of hiPSC-CM's post PDA-NP's treatment (5, 10, and 25 $\mu\text{g/mL}$). (B) Graph representing dose dependent fold-change in beat period of hiPSC-CM's post PDA-NPs treatment, ** $P < 0.01$, *** $P < 0.001$, **** $P < 0.0001$. (C) Graph representing fold-change in field potential duration in a dose dependent manner (5, 10, and 25 $\mu\text{g/mL}$), ** $P < 0.01$. (D, E, and F) Representative field potential duration of hiPSC-CM's treated with 5, 10, and 25 $\mu\text{g/mL}$ of PDA-NPs, respectively. Data represent Mean \pm SD. One-way ANOVA was performed followed by Dunnett's test for comparison with control.

concentrations of H_2O_2 as shown in Figure S5A–C and tested for free radical quenching efficacy (Figure S5D). It was observed that PDA-NPs retained the antioxidant potential even when degraded beyond 50%. These findings support the earlier published report suggesting that degraded PDA-NPs could be bioactive.¹⁷

The intracellular quenching of H_2O_2 by PDA-NPs was also assessed, and as shown in Figure 8C, a significant increase in intracellular H_2O_2 was observed when cells were exposed to 100 μM H_2O_2 . Whereas a significant inhibition in intracellular H_2O_2 was observed in PDA-NPs pretreated cells. Furthermore, in the current study, we have evaluated ATP production in cardiomyocytes post-PDA-NPs treatment. Interestingly, we observed that 10 $\mu\text{g/mL}$ PDA-NPs treatment significantly enhanced the ATP production in a time-dependent manner, as strikingly by the end of the 24 h time point a >15-fold increase in ATP was observed (Figure 8D). These findings support the use of PDA-NPs as a promising therapeutic agent for preserving the functioning and enhancing the ATP supply. Collectively, these

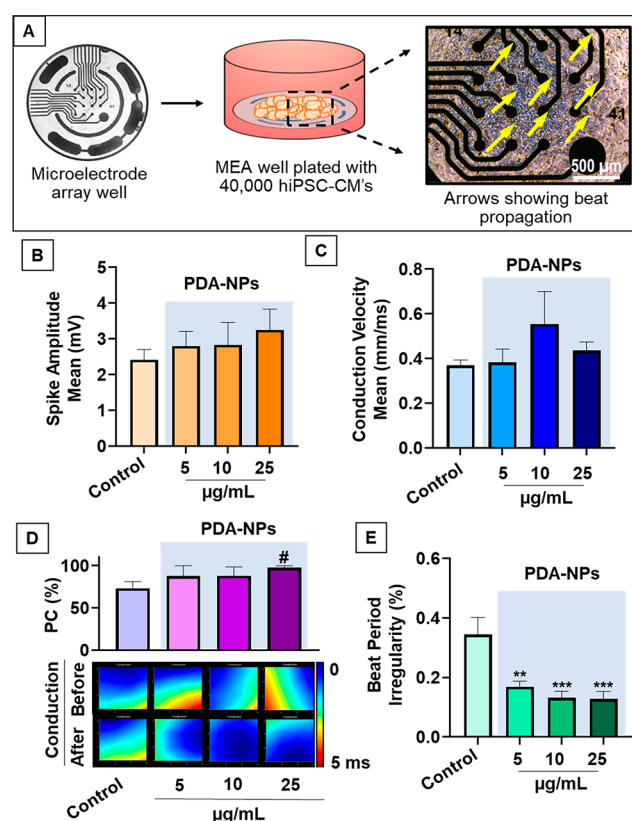


Figure 7. Electrophysiological assessment of hiPSC-CM's following PDA-NPs treatment. (A) Schematic representation of experimental design. (B) Graph representing modulation in spike amplitude of hiPSC-CM's treated with PDA-NPs (5, 10, and 25 $\mu\text{g/mL}$). (C) Graph representing conduction velocity of hiPSC-CM's monolayer treated with PDA-NPs (5, 10, and 25 $\mu\text{g/mL}$). (D) Graph representing propagation consistency of hiPSC-CM's monolayer treated with PDA-NPs (5, 10, and 25 $\mu\text{g/mL}$). # $P < 0.05$ (unpaired t test) and representative heat maps of MEA wells (4 \times 4 electrodes) demonstrating the beat propagation of hiPSC-CM's post PDA-NPs treatment. (E) Graph representing changes in beat period irregularity of hiPSC-CM's post PDA-NPs treatment, ** $P < 0.01$ *** $P < 0.001$, (5, 10, and 25 $\mu\text{g/mL}$). Data represent Mean \pm SEM. One-way ANOVA was performed followed by Dunnett's test for comparison with control.

findings demonstrate the multimodal effects of PDA-NPs on hiPSC-CMs like modulating the electrical properties of cardiomyocytes, enhancing ATP production and Redox buffering capacity.

The *in vitro* analysis of cardiomyocytes treated with PDA-NPs demonstrated a significant modulatory effect and enhanced the conduction velocity. To evaluate the effect of PDA-NPs on an isolated beating heart, the Langendorff heart perfusion setup was used as shown in Figure 9A. The isolated rat hearts treated with PDA-NPs showed a higher heart rate (Supporting video 1) with slight changes in ECG signal (Figure 9B and 9C). Furthermore, hemodynamic parameters were analyzed following the infusion of PDA-NPs (10 and 25 $\mu\text{g/mL}$). An immediate change in the LVSP, (\pm) dp/dt was observed. More importantly, when 10 $\mu\text{g/mL}$ was infused for 1 min, a gradual change in the hemodynamic parameters was noted which led to a 2-fold change by the end of 10 min post-infusion as shown in Figure 9D–9F. In contrast, the higher dose (25 $\mu\text{g/mL}$) showed an immediate change in all the hemodynamic parameters, but with a lesser magnitude compared to the 10 $\mu\text{g/mL}$ dose (Figure 9G–9I). These findings suggest that PDA-NPs could significantly enhance the

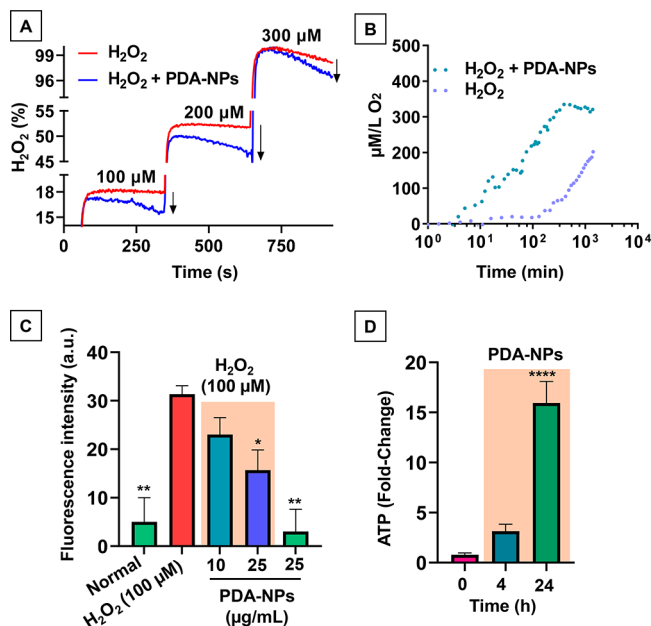


Figure 8. Antioxidant potential of PDA-NPs and modulation of cellular ATP levels. (A) Real-time H₂O₂ measurements and subsequent catalysis upon PDA-NPs (10 μg/mL) addition. (B) Graph representing real-time conversion of H₂O₂ to O₂ upon PDA-NPs addition (10 μg/mL). (C) PDA-NPs mediated quenching of intracellular H₂O₂. Data are represented as Mean ± SD. One-way ANOVA was performed followed by Dunnett's test for comparison with H₂O₂ treated group, **P* < 0.05, ***P* < 0.005. (D) Graph representing the fold-change in intracellular ATP levels before and after the PDA-NPs (10 μg/mL) treatment in a time dependent manner, *****P* < 0.0001. Data represent Mean ± SD. One-way ANOVA was performed followed by Dunnett's test for comparison with 0 h time point.

hemodynamic parameters possibly by exerting ionotropic effect in the isolated heart. It is worth noting that higher doses of PDA-NPs exerted a reversal phenomenon, similar to the biphasic response of cardiac drugs. Lastly, we also tested the cardiotoxic effect of PDA-NPs *in vivo*, as shown in Figure S6; following an i.v. injection a significant increase in the heart rate was observed at a dose of 1.6 mg/kg. Our findings confirm that PDA-NPs significantly modulate the activity of cardiomyocytes *in vitro* and in isolated perfused hearts *ex vivo* and *in vivo*.

Gene expression analysis of cardiomyocyte-associated genes was performed to determine the effect of PDA-NPs treatment on the structure and functionality of cardiomyocytes (Figure 10). hiPSC-CMs treated with 10 μg/mL of PDA-NPs and changes in the expression of different genes was assessed. We observed a significant increase in the expression of pluripotency marker, MYC (*p* = 0.0143) and an increase, although insignificant in another PSC marker NANOG. We also tested the expression of cardiac transcription factors, HCN1, NKX2.5, GATA4, and TBX5. Our results showed a significant increase in the expression of HCN1 while expression of GATA4 and TBX5 remained unchanged post-PDA-NP-treatment. There was an increase in expression of NKX2.5, although insignificant. Further, we evaluated the changes in expression of contractile genes like myosins and troponins. MYH6, α heavy chain, expression decreased with PDA-NPs treatment while no significant changes were seen in the expression of MYH7, β heavy chain. We also observed a significant increase in the expression of myosin light chains, MYL2 and MYL7. We also saw a modest increase in the expression of TNNI3 (*p* = 0.0562),

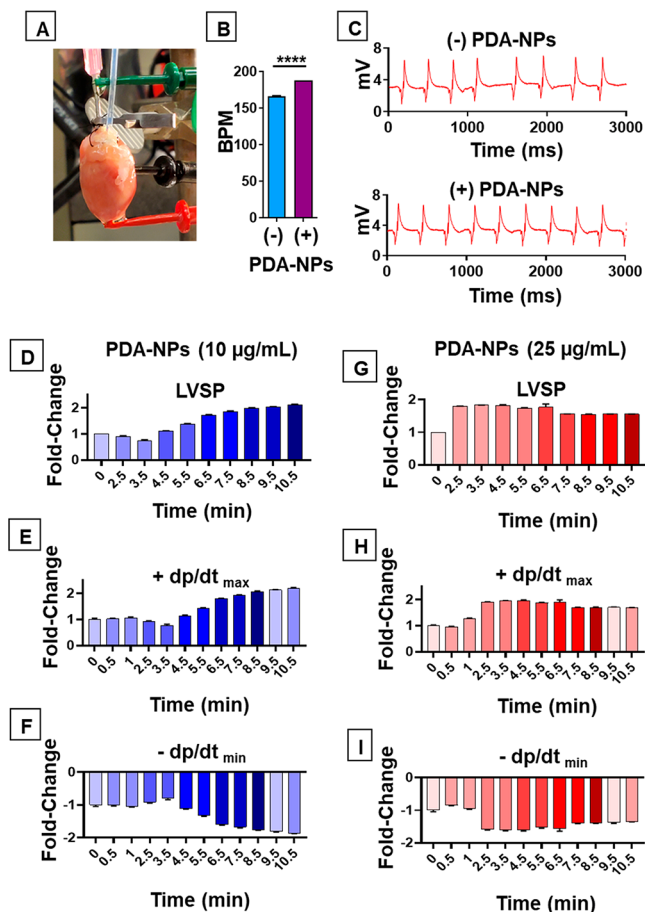


Figure 9. Modulation of hemodynamic parameters of isolated rat heart post PDA-NPs exposure. (A) Image representing the isolated rat heart mounted on Langendorff's heart perfusion setup mounted with ECG electrodes. (B) Graph representing modulation of heartbeat post PDA-NPs infusion (*****P* < 0.0001). (C) Graph representing the ECG changes in the isolated perfused heart with/without PDA-NPs treatment. (D, E, and F) Graph representing modulation of hemodynamic parameters LVSP, +dp/dt_{max}, +dp/dt_{min} following 10 μg/mL PDA-NPs for 1 min. (G, H, and I) Graph representing modulation of LVSP, +dp/dt_{max}, +dp/dt_{min} following 25 μg/mL PDA-NPs for 1 min. Data represent Mean ± SD. One-way ANOVA was performed followed by Dunnett's test for comparison with control.

the only detectable isoform of adult hearts. We have previously reported a similar expression pattern change during metabolic and functional maturation of hiPSC-CMs.³⁰ Furthermore, we also detected a modest increase in Connexin 43, encoded by GJA1 (*p* = 0.3707) and a significant increase in expression of Connexin 43, encoded by GJA5. This is consistent with an increase in electrical coupling and conductivity of hiPSC-CMs. Interestingly, consistent with the localization of PDA-NPs to mitochondria and increased intracellular ATP in the hiPSC-CMs, we observed a significant upregulation of PDHA1 and ACADM, a mitochondrial gene associated with ATP production. Taken together, our results showed a beneficial role in PDA-NP treatment of hiPSC-CMs including improved function and maturation and thereby a positive indication of their potential role in cardiac therapeutics.

Limitations and Future Directions. The major limitation in using PDA-NPs for cardiovascular applications is the nonspecific accumulation of nanoparticles in other organs. This would influence the effective dose needed for therapeutic

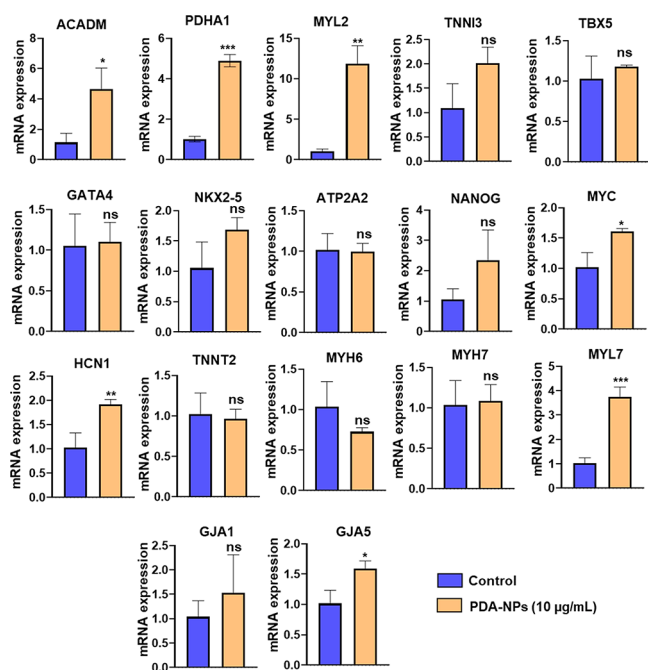


Figure 10. Graphical representation of fold-change mRNA expression in cardiac specific genes following the PDA-NPs treatment (10 µg/mL). Data are represented as Mean ± SD and were analyzed by performing unpaired *t* test, **P* < 0.01, ***P* < 0.001, ****P* < 0.0001.

effect. Although numerous studies have reported PDA-NPs to be safe, and our *in vitro* studies showed no negative effect on hiPSC-CM viability up to 2 weeks after PDA-NP treatment, it is still unclear whether long-term retention of these nanoparticles increases the risk of adverse effects. Moreover, the size of PDA-NPs has also been reported to influence the activity. Therefore, future studies focusing on establishing the pharmacokinetic profile of PDA-NPs and its effect due to variation in size are desirable. Furthermore, it would be worth exploring the effect of engineered PDA-NPs to minimize the retention and improve the clearance. Finally, the current study was only focused on evaluating the direct effect of PDA-NPs on hiPSC-CMs activity. However, mechanistic evaluation of PDA-NPs-mediated modulation of cellular activity needs further exploration.

CONCLUSIONS

In summary, we have demonstrated that the activity of hiPSC-derived cardiomyocytes could significantly be modulated by PDA-NPs. The multifaceted properties of PDA-NPs make them promising nanotherapy avenues for heart failure. PDA-NPs showed a drug-like effect on cardiomyocytes by enhancing cell contractility and conductivity. Furthermore, the intracellular mitochondrial targeting of PDA-NPs and enhanced ATP production demonstrate the potential of next-generation nanotherapeutics for treating failing hearts. The real-time catalysis of H₂O₂ and ROS quenching by PDA-NPs show the enzyme-like behavior of the nanoparticles, which could play a crucial role in cardioprotection. Additionally, PDA-NPs showed modulation of cardiac activity when tested on *ex vivo* isolated perfused hearts and *in vivo*. The improvement in hemodynamic functional parameters shows the bioactivity of PDA-NPs on the heart. Collectively, these findings imply that newer nanoparticles like PDA-NPs displaying multimodal potential could be used as promising cardiac nanomedicine therapeutics.

ASSOCIATED CONTENT

Supporting Information

The Supporting Information is available free of charge at <https://pubs.acs.org/doi/10.1021/acsami.2c12575>.

Characterization of PDA-NPs loaded with calcein (UV-vis and fluorescence spectroscopy), confocal image of PDA-NPs and isolated mitochondria, DPPH analysis of PDA-NPs, H₂O₂ mediated cell injury, Accelerated degradation studies of PDA-NPs, *in vivo* assessment of PDA-NPs. (PDF)

Video of isolated rat hearts treated with PDA-NPs showing a slightly higher heart rate (MP4)

AUTHOR INFORMATION

Corresponding Author

Mahmood Khan – Department of Emergency Medicine, College of Medicine, The Ohio State University, Columbus, Ohio 43210, United States; Department of Physiology and Cell Biology and Davis Heart and Lung Research Institute, The Ohio State University, Columbus, Ohio 43210, United States; orcid.org/0000-0003-3430-374X; Phone: 614-688-7803; Email: mahmood.khan@osumc.edu

Authors

Syed Baseeruddin Alvi – Department of Emergency Medicine, College of Medicine, The Ohio State University, Columbus, Ohio 43210, United States

Divya Sridharan – Department of Emergency Medicine, College of Medicine, The Ohio State University, Columbus, Ohio 43210, United States

Mahmoud T. Shalaan – Department of Emergency Medicine, College of Medicine, The Ohio State University, Columbus, Ohio 43210, United States

Shridhar K. Sanghvi – Department of Physiology and Cell Biology, The Ohio State University, Columbus, Ohio 43210, United States

Muhamad Mergaye – Department of Emergency Medicine, College of Medicine, The Ohio State University, Columbus, Ohio 43210, United States

Uzair Ahmed – Department of Emergency Medicine, College of Medicine, The Ohio State University, Columbus, Ohio 43210, United States

Sarah K. Mikula – Center for Electron Microscopy and Analysis, The Ohio State University, Columbus, Ohio 43210, United States

Harpreet Singh – Department of Physiology and Cell Biology and Davis Heart and Lung Research Institute, The Ohio State University, Columbus, Ohio 43210, United States

Complete contact information is available at: <https://pubs.acs.org/10.1021/acsami.2c12575>

Author Contributions

S.B.A. and D.S. worked on design, conceptualization, data collection, data analysis, review of the study. M.T.S. performed H₂O₂ and O₂ measurements, S.K.S. performed calcium imaging, M.M. performed MEA data analysis, U.A. performed data analysis of calcium imaging, S.K.M. performed TEM imaging of cells, H.S. performed isolated mitochondrial binding analysis, and M.K. performed the *ex vivo* and *in vivo* experiments.

Author Contributions

#S.B.A. and D.S. contributed equally.

Notes

The authors declare no competing financial interest.

ACKNOWLEDGMENTS

The authors would like to acknowledge CEMAS and CMIF for the imaging facility. We would also like to thank Dr. Luis Rodriguez-Saona (Department of Food Sciences and Technology) at The Ohio State University for FTIR analysis and Dr. Yizhou Dong from the College of Pharmacy at The Ohio State University for Zeta-Potential analysis. We thank Lisa Baer from Dr. Kristin Stanford's lab (Department of Physiology) for helping us with ATP measurements. We would also like to acknowledge the grant support from NIH to M.K. (HL136232). Figure ¹ was created with BioRender.com.

REFERENCES

- (1) Murphy, S. P.; Ibrahim, N. E.; Januzzi, J. L., Jr. Heart Failure With Reduced Ejection Fraction: A Review. *JAMA* **2020**, *324* (5), 488–504.
- (2) Dokainish, H.; Teo, K.; Zhu, J.; Roy, A.; AlHabib, K. F.; ElSayed, A.; Palileo-Villaneuva, L.; Lopez-Jaramillo, P.; Karaye, K.; Yusoff, K.; Orlandini, A.; Sliwa, K.; Mondo, C.; Lanus, F.; Prabhakaran, D.; Badr, A.; Elmaghawry, M.; Damasceno, A.; Tibazarwa, K.; Belley-Cote, E.; Balasubramanian, K.; Islam, S.; Yacoub, M. H.; Huffman, M. D.; Harkness, K.; Grinvalds, A.; McKelvie, R.; Bangdiwala, S. I.; Yusuf, S.; Investigators, I.-C. Global mortality variations in patients with heart failure: results from the International Congestive Heart Failure (INTER-CHF) prospective cohort study. *Lancet Glob Health* **2017**, *5* (7), e665–e672.
- (3) Severino, P.; D'Amato, A.; Pucci, M.; Infusino, F.; Adamo, F.; Birtolo, L. I.; Netti, L.; Montefusco, G.; Chimenti, C.; Lavallo, C.; Maestrini, V.; Mancone, M.; Chilian, W. M.; Fedele, F. Ischemic Heart Disease Pathophysiology Paradigms Overview: From Plaque Activation to Microvascular Dysfunction. *Int. J. Mol. Sci.* **2020**, *21* (21), 8118.
- (4) Bugger, H.; Pfeil, K. Mitochondrial ROS in myocardial ischemia reperfusion and remodeling. *Biochim Biophys Acta Mol. Basis Dis* **2020**, *1866* (7), 165768.
- (5) DeLeon-Pennell, K. Y.; Meschiari, C. A.; Jung, M.; Lindsey, M. L. Matrix Metalloproteinases in Myocardial Infarction and Heart Failure. *Prog. Mol. Biol. Transl. Sci.* **2017**, *147*, 75–100.
- (6) Ho, P. M.; Spertus, J. A.; Masoudi, F. A.; Reid, K. J.; Peterson, E. D.; Magid, D. J.; Krumholz, H. M.; Rumsfeld, J. S. Impact of medication therapy discontinuation on mortality after myocardial infarction. *Arch Intern Med.* **2006**, *166* (17), 1842–7.
- (7) Ingwall, J. S.; Weiss, R. G. Is the failing heart energy starved? On using chemical energy to support cardiac function. *Circ. Res.* **2004**, *95* (2), 135–45.
- (8) Neubauer, S. The failing heart—an engine out of fuel. *N Engl J. Med.* **2007**, *356* (11), 1140–51.
- (9) Ingwall, J. S. Energy metabolism in heart failure and remodeling. *Cardiovasc. Res.* **2008**, *81* (3), 412–9.
- (10) Tromp, J.; Ouwerkerk, W.; van Veldhuisen, D. J.; Hillege, H. L.; Richards, A. M.; van der Meer, P.; Anand, I. S.; Lam, C. S. P.; Voors, A. A. A Systematic Review and Network Meta-Analysis of Pharmacological Treatment of Heart Failure With Reduced Ejection Fraction. *JACC Heart Fail* **2022**, *10* (2), 73–84.
- (11) Brown, D. A.; Perry, J. B.; Allen, M. E.; Sabbah, H. N.; Stauffer, B. L.; Shaikh, S. R.; Cleland, J. G.; Colucci, W. S.; Butler, J.; Voors, A. A.; Anker, S. D.; Pitt, B.; Pieske, B.; Filippatos, G.; Greene, S. J.; Gheorghiade, M. Expert consensus document: Mitochondrial function as a therapeutic target in heart failure. *Nat. Rev. Cardiol* **2017**, *14* (4), 238–250.
- (12) Antoniadou, C.; Demosthenous, M.; Reilly, S.; Margaritis, M.; Zhang, M. H.; Antonopoulos, A.; Marinou, K.; Nahar, K.; Jayaram, R.; Tousoulis, D.; Bakogiannis, C.; Sayeed, R.; Triantafyllou, C.; Koumallos, N.; Psarros, C.; Miliou, A.; Stefanadis, C.; Channon, K. M.; Casadei, B. Myocardial redox state predicts in-hospital clinical outcome after cardiac surgery effects of short-term pre-operative statin treatment. *J. Am. Coll. Cardiol* **2012**, *59* (1), 60–70.
- (13) Knowlton, A. A.; Chen, L.; Malik, Z. A. Heart failure and mitochondrial dysfunction: the role of mitochondrial fission/fusion abnormalities and new therapeutic strategies. *J. Cardiovasc Pharmacol* **2014**, *63* (3), 196–206.
- (14) Sabbah, H. N. Targeting the Mitochondria in Heart Failure: A Translational Perspective. *JACC Basic Transl Sci.* **2020**, *5* (1), 88–106.
- (15) O'Connor, N. A.; Syed, A.; Wong, M.; Hicks, J.; Nunez, G.; Jitianu, A.; Siler, Z.; Peterson, M. Polydopamine Antioxidant Hydrogels for Wound Healing Applications. *Gels* **2020**, *6* (4), 39.
- (16) Zhang, Y.; Ren, X.; Wang, Y.; Chen, D.; Jiang, L.; Li, X.; Li, T.; Huo, M.; Li, Q. Targeting Ferroptosis by Polydopamine Nanoparticles Protects Heart against Ischemia/Reperfusion Injury. *ACS Appl. Mater. Interfaces* **2021**, *13* (45), 53671–53682.
- (17) Jin, L.; Yuan, F.; Chen, C.; Wu, J.; Gong, R.; Yuan, G.; Zeng, H.; Pei, J.; Chen, T. Degradation Products of Polydopamine Restrained Inflammatory Response of LPS-Stimulated Macrophages Through Mediation TLR-4-MYD88 Dependent Signaling Pathways by Antioxidant. *Inflammation* **2019**, *42* (2), 658–671.
- (18) Li, J.; Hou, W.; Lin, S.; Wang, L.; Pan, C.; Wu, F.; Liu, J. Polydopamine Nanoparticle-Mediated Dopaminergic Immunoregulation in Colitis. *Adv. Sci. (Weinh)* **2022**, *9* (1), No. 2104006.
- (19) Kwon, I. S.; Bettinger, C. J. Polydopamine Nanostructures as Biomaterials for Medical Applications. *J. Mater. Chem. B* **2018**, *6* (43), 6895–6903.
- (20) Hajipour, M. J.; Mehrani, M.; Abbasi, S. H.; Amin, A.; Kassaian, S. E.; Garbern, J. C.; Caracciolo, G.; Zanganeh, S.; Chitsazan, M.; Aghaverdi, H.; Kamali Shahri, S. M.; Ashkarran, A.; Raoufi, M.; Bauser-Heaton, H.; Zhang, J.; Muehlschlegel, J. D.; Moore, A.; Lee, R. T.; Wu, J. C.; Serpooshan, V.; Mahmoudi, M. Nanoscale Technologies for Prevention and Treatment of Heart Failure: Challenges and Opportunities. *Chem. Rev.* **2019**, *119* (21), 11352–11390.
- (21) Kumar, N.; Sridharan, D.; Palaniappan, A.; Dougherty, J. A.; Czirok, A.; Isai, D. G.; Mergaye, M.; Angelos, M. G.; Powell, H. M.; Khan, M. Scalable Biomimetic Coaxial Aligned Nanofiber Cardiac Patch: A Potential Model for "Clinical Trials in a Dish". *Front Bioeng Biotechnol* **2020**, *8*, 567842.
- (22) Nieto, C.; Marcelo, G.; Vega, M.; Martin Del Valle, E. M. Antineoplastic behavior of polydopamine nanoparticles prepared in different water/alcohol media. *Colloids Surf. B Biointerfaces* **2021**, *199*, 111506.
- (23) P.S. R.; Alvi, S. B.; Begum, N.; Veeresh, B.; Rengan, A. K. Self-Assembled Fluorosome-Polydopamine Complex for Efficient Tumor Targeting and Commingled Photodynamic/Photothermal Therapy of Triple-Negative Breast Cancer. *Biomacromolecules* **2021**, *22* (9), 3926–3940.
- (24) Gholami Derami, H.; Gupta, P.; Weng, K. C.; Seth, A.; Gupta, R.; Silva, J. R.; Raman, B.; Singamaneni, S. Reversible Photothermal Modulation of Electrical Activity of Excitable Cells using Polydopamine Nanoparticles. *Adv. Mater.* **2021**, *33* (32), No. 2008809.
- (25) Khan, M.; Xu, Y.; Hua, S.; Johnson, J.; Belevych, A.; Janssen, P. M.; Gyorke, S.; Guan, J.; Angelos, M. G. Evaluation of Changes in Morphology and Function of Human Induced Pluripotent Stem Cell Derived Cardiomyocytes (hiPSC-CMs) Cultured on an Aligned-Nanofiber Cardiac Patch. *PLoS One* **2015**, *10* (5), No. e0126338.
- (26) Sridharan, D.; Palaniappan, A.; Blackstone, B. N.; Dougherty, J. A.; Kumar, N.; Seshagiri, P. B.; Sayed, N.; Powell, H. M.; Khan, M. In situ differentiation of human-induced pluripotent stem cells into functional cardiomyocytes on a coaxial PCL-gelatin nanofibrous scaffold. *Mater. Sci. Eng. C Mater. Biol. Appl.* **2021**, *118*, 111354.
- (27) Sanghvi, S.; Sztejn, K.; Ponnalagu, D.; Sridharan, D.; Lam, A.; Hansra, L.; Chaudhury, A.; Majumdar, U.; Kohut, A. R.; Gururaja Rao, S.; Khan, M.; Garg, V.; Singh, H. Inhibition of BKCa channels protects neonatal hearts against myocardial ischemia and reperfusion injury. *Cell Death Discov* **2022**, *8* (1), 175.
- (28) Ponnalagu, D.; Hussain, A. T.; Thanawala, R.; Meka, J.; Bednarczyk, P.; Feng, Y.; Szewczyk, A.; Gururaja Rao, S.; Bopassa, J. C.; Khan, M.; Singh, H. Chloride channel blocker IAA-94 increases

myocardial infarction by reducing calcium retention capacity of the cardiac mitochondria. *Life Sci.* **2019**, *235*, 116841.

(29) Singh, H.; Lu, R.; Bopassa, J. C.; Meredith, A. L.; Stefani, E.; Toro, L. MitoBK(Ca) is encoded by the Kcnma1 gene, and a splicing sequence defines its mitochondrial location. *Proc. Natl. Acad. Sci. U. S. A.* **2013**, *110* (26), 10836–41.

(30) Kumar, N.; Dougherty, J. A.; Manring, H. R.; Elmadbouh, I.; Mergaye, M.; Czirok, A.; Greta Isai, D.; Belevych, A. E.; Yu, L.; Janssen, P. M. L.; Fadda, P.; Gyorke, S.; Ackermann, M. A.; Angelos, M. G.; Khan, M. Assessment of temporal functional changes and miRNA profiling of human iPSC-derived cardiomyocytes. *Sci. Rep.* **2019**, *9* (1), 13188.

(31) Liu, H.; Qu, X.; Tan, H.; Song, J.; Lei, M.; Kim, E.; Payne, G. F.; Liu, C. Role of polydopamine's redox-activity on its pro-oxidant, radical-scavenging, and antimicrobial activities. *Acta Biomater.* **2019**, *88*, 181–196.

(32) Mastore, M.; Kohler, L.; Nappi, A. J. Production and utilization of hydrogen peroxide associated with melanogenesis and tyrosinase-mediated oxidations of DOPA and dopamine. *FEBS J.* **2005**, *272* (10), 2407–15.

(33) An, J. M.; Ju, Y.; Kim, J. H.; Lee, H.; Jung, Y.; Kim, J.; Kim, Y. J.; Kim, J.; Kim, D. A metastasis suppressor Pt-dendrimer nanozyme for the alleviation of glioblastoma. *J. Mater. Chem. B* **2021**, *9* (19), 4015–4023.

(34) Singh, G.; Sridharan, D.; Khan, M.; Seshagiri, P. B. Mouse embryonic stem cell-derived cardiomyocytes cease to beat following exposure to monochromatic light: association with increased ROS and loss of calcium transients. *Am. J. Physiol. Cell Physiol.* **2019**, *317* (4), C725–C736.

(35) Kutala, V. K.; Khan, M.; Mandal, R.; Ganesan, L. P.; Tridandapani, S.; Kalai, T.; Hideg, K.; Kuppusamy, P. Attenuation of myocardial ischemia-reperfusion injury by trimetazidine derivatives functionalized with antioxidant properties. *J. Pharmacol. Exp. Ther.* **2006**, *317* (3), 921–8.

(36) Yang, Y.; Zhang, Y.; Chai, R.; Gu, Z. A Polydopamine-Functionalized Carbon Microfibrous Scaffold Accelerates the Development of Neural Stem Cells. *Front. Bioeng. Biotechnol.* **2020**, *8*, 616.

(37) Ye, G.; Wen, Z.; Wen, F.; Song, X.; Wang, L.; Li, C.; He, Y.; Prakash, S.; Qiu, X. Mussel-inspired conductive Ti2C-cryogel promotes functional maturation of cardiomyocytes and enhances repair of myocardial infarction. *Theranostics* **2020**, *10* (5), 2047–2066.

(38) Tang, Y.; Tan, Y.; Lin, K.; Zhu, M. Research Progress on Polydopamine Nanoparticles for Tissue Engineering. *Front. Chem.* **2021**, *9*, 727123.

(39) Kim, S.; Jang, L. K.; Jang, M.; Lee, S.; Hardy, J. G.; Lee, J. Y. Electrically Conductive Polydopamine-Polypyrrole as High Performance Biomaterials for Cell Stimulation in Vitro and Electrical Signal Recording in Vivo. *ACS Appl. Mater. Interfaces* **2018**, *10* (39), 33032–33042.

(40) Kim, R.; Nam, Y. Polydopamine-doped conductive polymer microelectrodes for neural recording and stimulation. *J. Neurosci. Methods* **2019**, *326*, 108369.

(41) Battaglini, M.; Marino, A.; Carmignani, A.; Tapeinos, C.; Cauda, V.; Ancona, A.; Garino, N.; Vighetto, V.; La Rosa, G.; Sinibaldi, E.; Ciofani, G. Polydopamine Nanoparticles as an Organic and Biodegradable Multitasking Tool for Neuroprotection and Remote Neuronal Stimulation. *ACS Appl. Mater. Interfaces* **2020**, *12* (32), 35782–35798.

(42) Singh, H.; Lu, R.; Rodriguez, P. F.; Wu, Y.; Bopassa, J. C.; Stefani, E.; Toro, L. Visualization and quantification of cardiac mitochondrial protein clusters with STED microscopy. *Mitochondrion* **2012**, *12* (2), 230–6.

(43) Millard, D.; Dang, Q.; Shi, H.; Zhang, X.; Strock, C.; Kraushaar, U.; Zeng, H.; Levesque, P.; Lu, H. R.; Guillon, J. M.; Wu, J. C.; Li, Y.; Luerman, G.; Anson, B.; Guo, L.; Clements, M.; Abassi, Y. A.; Ross, J.; Pierson, J.; Gintant, G. Cross-Site Reliability of Human Induced Pluripotent stem cell-derived Cardiomyocyte Based Safety Assays Using Microelectrode Arrays: Results from a Blinded CiPA Pilot Study. *Toxicol. Sci.* **2018**, *164* (2), 550–562.

(44) Seddon, M.; Looi, Y. H.; Shah, A. M. Oxidative stress and redox signalling in cardiac hypertrophy and heart failure. *Heart* **2007**, *93* (8), 903–7.

(45) Fu, Y.; Zhang, J.; Wang, Y.; Li, J.; Bao, J.; Xu, X.; Zhang, C.; Li, Y.; Wu, H.; Gu, Z. Reduced polydopamine nanoparticles incorporated oxidized dextran/chitosan hybrid hydrogels with enhanced antioxidative and antibacterial properties for accelerated wound healing. *Carbohydr. Polym.* **2021**, *257*, 117598.

(46) Bao, X.; Zhao, J.; Sun, J.; Hu, M.; Yang, X. Polydopamine Nanoparticles as Efficient Scavengers for Reactive Oxygen Species in Periodontal Disease. *ACS Nano* **2018**, *12* (9), 8882–8892.

(47) Wei, Y.; Zhu, M.; Li, S.; Hong, T.; Guo, X.; Li, Y.; Liu, Y.; Hou, X.; He, B. Engineered Biomimetic Nanoplatfrom Protects the Myocardium Against Ischemia/Reperfusion Injury by Inhibiting Pyroptosis. *ACS Appl. Mater. Interfaces* **2021**, *13* (29), 33756–33766.